# Association of Ionized Polymer Micelles with Oppositely Charged Polyelectrolytes

**C. Simmons,[†] S. E. Webber,*[,†] and E. B. Zhulina[†,‡]**

*Department of Chemistry and Biochemistry, and Texas Materials Institute, University of Texas at Austin, Austin, Texas 78712, and Institute of Macromolecular Compounds, of the Russian Academy of Sciences, 199004 St. Petersburg, Russia*

*Received March 5, 2001; Revised Manuscript Received May 3, 2001*

ABSTRACT: We consider the equilibrium structure of the complex formed by an ionized starlike polymer micelle with oppositely charged polyion. The charges on both the micelle and polyion are quenched, and the complex is immersed in a salt-free aqueous solution. Analytical and numerical self-consistent-field (SCF) models are employed to describe the properties of such a complex. Our findings indicate that the micelle−polyion complex is essentially electroneutral as a whole and that the polyion replaces almost all small counterions within the micelle corona. The structure of the complex is governed by the effective second and third virial coefficients of monomer−monomer interactions and is much more compact than original ionized micelle. Furthermore, the structure of the complex is predicted to be insensitive to the molecular weight of the polyion. The effective virial coefficients can be mediated by variations in the solvent quality, the degree of ionization, and the incompatibility of the branches of the micelle and polyion. We derive the diagram of the states of the complex and delineate the range of its thermodynamic stability. The results of numerical SCF calculations are in reasonable agreement with the analytical predictions. It is also found that the detailed distribution of the polyion charge has only a minor effect on the overall structure of the complex.

## I. Introduction

Electrostatic interactions between oppositely charged objects drive them to associate and to form complexes of various morphologies. The controlled complexation of charged macromolecules plays an important role in various fields of science and technology. For example, association of oppositely charged polymers into multilayer structures gives rise to thin conductive films for microelectronics,[1,2] whereas adsorption of polyelectrolytes on colloid particles governs the stability and flocculation of dispersions[3] In biology, association of DNA with cationic proteins and liposomes plays a central role in gene reproduction and therapy [4,5] There have been several recent reports of the formation of micellar structures from the interaction of two oppositely charged block copolymers.[6]

In our study we focus on the association behavior of ionized polymer micelles with oppositely charged linear polyions. Charged polymer micelles have been a subject of intensive experimental and theoretical investigations during the past decade.[7−11] Many of the charged micelle systems exhibit high aggregation stability in a wide range of conditions because of their glassy core while being resistant against aggregation by virtue of the corona charge and steric stabilization. This makes them attractive candidates for targeted drug delivery and other biomedical applications.[12] The structure and size of the charged micelle coronas are governed by both the long-range electrostatic forces and the sort-range van der Waals interactions. As a result, the coronas of such micelles are more extended and exhibit a much different internal organization than their neutral analogues.[13] The intracorona electrostatic interactions can be mediated by additions of low molecular weight salt or oppositely charged macroions. When oppositely charged polymers are added in the solution, they can penetrate in the corona of the micelle and give rise to micelle−polyion complexes. Recent experiments clearly indicate that charged micelles prepared from PS-*b*-PVP block copolymers can form water-soluble complexes with negatively charged sulfonated polystyrene (PSS).[14] The mass ratio of PSS per micelle was shown to depend weakly on the molecular weight of PSS and the ionic strength of the solution. An interesting feature of such a complex is huge mass overcompensation. That is, the mass ratio of bound PSS and PS-*b*-PVP micelle could be much higher than unity.[14]

The goal of this paper is to examine how the structure and properties of a micelle−polyion complex in a salt-free solution depend on the molecular parameters of each constituent. In section II we describe the model of the complex. We then apply two theoretical methods to investigate the features of such a complex. In section III, we develop an analytical self-consistent-field theory to describe the internal structure of a micelle interacting with the polyion and derive the diagram of states for such a complex. In section IV we supplement our analytical findings with the results of a numerical self-consistent-field (SCF) model which employs the Scheutjens−Fleer formalism generalized for charged species on the Poisson−Boltzmann level.[15] Finally, in section V we discuss the results and summarize our conclusions.

## II. Model

We consider a spherical polymer micelle formed by AB diblock copolymers with a charged soluble block. The micelle is immersed in solvent (water). The core of such a micelle contains the insoluble block B whereas the corona is formed by the charged blocks A which provide the solubility of the micelle in the solution. At equilibrium the aggregation number $f$ (i.e., the number of

[†] University of Texas at Austin.
[‡] Russian Academy of Sciences.

10.1021/ma010399r CCC: $20.00 
Published on Web 06/06/2001

diblocks per micelle) is governed by the molecular parameters of the blocks and the ionic strength of the solution.[7] However, under experimental conditions, the micelles often demonstrate"nonequilibrium" behavior. This is conventionally attributed to the "freezing " of the core of micelle. We adopt such a picture and assume below that the aggregation number $f$ in the micelle is fixed and remains unchanged in the process of complexation between the micelle and the polyions. This is the case for the physical system of micelles formed from protonated PS-*b*-PVP.[14] It is not possible to protonate a polymer micelle of this type until the "frozen" neutral micelle has been formed in mixed organic solvents. Therefore, there is no effect of the charge on the corona on $f$.

We assume that the overall size of the micelle ($H$) is noticeably larger than radius of the core ($R$), and therefore the micelle demonstrates "starlike" behavior. We let $N$ be the number of monomers of size $a$ in each branch of the micelle and $\alpha$ be the degree of ionization. The charge on each branch $q = \alpha N$ is quenched. That is, $\alpha$ does not depend on the distance from the core and on the variations in the ionic strength in the surrounding solution. The total number of charges on the micelle is $Q = fq = f\alpha N$. In the absence of oppositely charged polyions, the starlike micelle also contains mobile counterions. For strongly charged micelles with $Q \gg H/l_B$ ($l_B = e^2/\epsilon kT$ is the Bjerrum length, where $e$ is the elementary charge and $\epsilon$ is the dielectric constant of the solution), almost all of the counterions are trapped inside the micelle. Under these conditions, the corona is swollen by the osmotic pressure of the counterions, and its thickness scales as[16]

$$H = a\alpha^{1/2}N \tag{1}$$

The counterions are "trapped" inside the micelle when the aggregation number is large enough,

$$f \gg a/(l_B\alpha^{1/2}) \tag{2}$$

Below we assume that inequality (2) is always fulfilled.

We focus on a salt-free solution of micelles (no excess low molecular weight salt is added in the solution). The micelle solution is considered to be so dilute that the addition of oppositely charged macroions leads to the formation of single micelle complexes only (e.g., formation of multimicelle aggregates is neglected).

When oppositely charged polyions (with charge density $\beta$) are added to the solution, they preferentially displace counterions that are trapped inside the micelle because of the total gain in the translational entropy (on the order of $QkT$ per micelle). The entropy losses due to penetration of long polyions inside the micelle are small with respect to the entropy gain of mobile counterions, and we neglect this factor. In the following, we assume that the branches of both the micelle and the polyions are weakly charged ($\alpha$ and $\beta \ll 1$, while still satisfying eq 2) and that both corona-forming polymers and polyions are intrinsically flexible (that is, in the uncharged state the Kuhn length of the backbone of each polymer is comparable to the size of a monomer). The weak charging and the flexibility ensure the local Gaussian statistics of the chains, and under these conditions the electrostatic stiffening of the chains is negligible.

Electrostatic interactions between the branches of the micelle corona and the polyions lead to formation of a complex. We denote the average density profiles of the corona and polyions by $c(x)$ and $n(x)$, respectively ($x$ is the distance from the core−corona interface). The distribution of the overall charge due to the corona and polyion in the complex is then given by $e\rho(x) = e[\alpha c(x) - \beta n(x)]$. Note that the charge on both polyelectrolytes is assumed to be homogeneously distributed along the polymer backbone, which also is the assumption used for the SCF calculations to be discussed later.

In addition to the electrostatic forces, the monomers of the micelle corona and polyion experience short-range nonelectrostatic interactions. We assume for simplicity that the thermodynamic quality of the solvent with respect to the nonelectrostatic interactions is the same for both the corona of the micelle and the polyion, and we describe them through the second ($v$) and the third ($w$) virial coefficients of monomer−monomer interactions. In the framework of the Flory theory of polymer solutions, the density of the free energy of such interactions is given by[17]

$$f_{mix}/kT = v[n(x) + c(x)]^2 + w[n(x) + c(x)]^3 + \chi c(x)\, n(x) \tag{3}$$

where $v/a^3 = {}^1/_2 - \chi_{ps}$, and $\chi_{ps}$ and $\chi$ are the respective Flory−Huggins parameters of monomer−solvent and monomer−monomer interactions. Under conditions of a good or $\Theta$ solvent ($v > 0$ or 0, respectively), the nonelectrostatic interactions are repulsive and lead to the stretching of the branches of micelle even in the absence of the electrostatic interactions. In a poor solvent ($v < 0$), the attraction between monomers can lead to the collapse of the corona of micelle. In the salt-free solution, collapse of the starlike corona occurs as an abrupt transition. The transition point is specified by the condition $v_t = -a^3\alpha^{-1/2}$.[16] Above the transition point, $v > v_t$, the corona is swollen by the osmotic pressure of counterions, and its size ($H$) is given by eq 1. Below the transition point, $v < v_t$, the nonelectrostatic attraction dominates, and the corona of the micelle shrinks. As a result, the solution of micelles becomes unstable. Below we focus on the range of solvent strength corresponding to the values of $v > v_t = -a^3\alpha^{-1/2}$.

## III. Analytical Self-Consistent-Field Theory

**A. Free Energy of the Complex $\Delta\Phi$.** We start with formulating the expression for the free energy $\Delta\Phi$ of the micelle−polyion complex in a salt-free solution. In this case, it is reasonable to assume that the mobile counterions are totally substituted by the polyions, and the free energy $\Delta\Phi$ consists of the following contributions:

$$\Delta\Phi = \Delta W_{el} + \Delta F_{mix} + \Delta F_{str} \tag{4}$$

Here, $\Delta W_{el}$ is the electrostatic energy due to the charge $\rho(x)$ distributed within the corona of micelle, $\Delta F_{mix}$ is the free energy of nonelectrostatic interactions, and $\Delta F_{str}$ is the free energy of stretching of the branches. As noted above, the translational entropy of the polyions within the micelle is neglected in our considerations.

**1. Electrostatic Energy.** The electrostatic contribution to the total free energy of the complex yields

$$\Delta W_{el}/kT = 1/(8\pi kT)\int_V \epsilon E^2\, dV \tag{5}$$

where $E$ is the electric field and integration is carried

over the volume $V$ of the complex. For the spherical symmetry of the complex the Gauss theorem relates the electric field $E$ to the charge distribution $\rho(x)$ as

$$E(r) = e/(\epsilon r^2) \int_R^r x^2[\alpha c(x) - \beta n(x)]\, dx \quad (6)$$

By substituting the expression for $E(r)$ into eq 5, we find

$$\Delta W_{el}/kT = l_B/2 \int_R^H r^{-2}\, dr\{\int_R^r x^2\, dx[\alpha c(x) - \beta n(x)]\}^2 \quad (7)$$

**2. Nonelectrostatic Interactions.** The contribution due to the nonelectrostatic interactions between monomers yields

$$\Delta F_{mix}/kT = 4\pi \int_R^H x^2\{v[n(x) + c(x)]^2 + w[n(x) + c(x)]^3 + \chi c(x)\, n(x)\}\, dx \quad (8)$$

where the integration is carried over the volume of the corona. We note that according to eq 8 both $v$ and $\chi$ have the dimensions of $a^3$ whereas $w$ scales as $a^6$.

**3. Stretching of Branches.** Finally, the last contribution to the free energy of the complex accounts for the nonuniform stretching of branches in the micelle. We assume that all the free ends of the corona chains are localized at the outer edge of the micelle and that the branches are stretched with respect to their Gaussian size. Under these conditions, the most probable location $x$ of the $p$th monomer of the branch could be specified by the "trajectory", $x = x(p)$.[18] The relationship between the local stretching of the chains ($dx/dp$) at distance $x$ from the center of micelle and the concentration of polymer units $c(x)$ yields

$$c(x) = f\, dp/(4\pi x^2\, dx) \quad (9)$$

Then the local stretching of the chains is given by

$$dx/dp = f/[4\pi x^2 c(x)] \quad (10)$$

Correspondingly, the elastic free energy due to the stretching of branches can be represented as[18]

$$\Delta F_{str}/kT = 3f/(2a^2) \int_R^H (dx/dp)\, dx = 3f^2/8\pi a^2 \int_R^H 1/[c(x)x^2]\, dx \quad (11)$$

**B. Minimization of the Free Energy $\Delta\Phi$.** We now must minimize the total free energy $\Delta\Phi$ with respect to the two unknown functions $c(x)$ and $n(x)$ under conditions of conservation of the total amount of polymer in the corona of the micelle,

$$4\pi \int_R^H c(x)x^2\, dx = fN \quad (12)$$

and of the total amount $M$ of polyion in the micelle,

$$4\pi \int_R^H n(x)x^2\, dx = M \quad (13)$$

The details of minimization procedure are collected in the Appendix. As is demonstrated in the Appendix, the electrostatic attraction between oppositely charged polymers (the corona-forming blocks and the polyion) is much stronger than the nonelectrostatic repulsion between monomers, and under a wide range of conditions, the complex is almost electroneutral locally,

$$\alpha c(x) \approx \beta n(x) \quad (14)$$

The electroneutrality condition in eq 14 is the basic approximation of our analytical model. It allows us to envision the micelle−polyion complex as a neutral system with the renormalized virial coefficients of monomer−monomer interactions. By substituting eq 14 in eq 3 for the density of the free energy of nonelectrostatic interactions, we obtain

$$\Delta f_{mix}/kT = v[(1 + \alpha/\beta)^2 + \alpha\chi/\beta]c(x)^2 + w(1 + \alpha/\beta)^3 c(x)^3 = v_{eff}c(x)^2 + w_{eff}c(x)^3 \quad (15)$$

where the effective second virial coefficient, $v_{eff}$, is given by

$$v_{eff} = v[(1 + \alpha/\beta)^2 + \alpha\chi/\beta] \quad (16)$$

whereas the effective third virial coefficient yields

$$w_{eff} = w(1 + \alpha/\beta)^3 \quad (17)$$

The local electroneutrality approximation (eq 14) makes it possible to substitute the original functional for the free enrgy, $\Delta\Phi$ (eqs 4, 7, 8, and 11) by the approximate functional which depends only on the local concentration of polymer $c(x)$,

$$\Delta\Phi/kT \approx 4\pi \int_R^H x^2 g\{c(x)\}\, dx = 4\pi \int_R^H x^2\{v_{eff}c(x)^2 + w_{eff}c(x)^3 + 3f^3/[32\pi^2 a^2 c(x)x^4]\}\, dx \quad (18)$$

Here, $g\{c(x)\}$ is the density of the free energy in the complex in framework of the local electroneutrality approximation. Equation 18 is equivalent to the corresponding equation for neutral spherical brushes or starlike polymers.[19] We now exploit this equivalence and formulate below the results that follow from eq 18.

## IV. Results

**A. Polymer Density Profile $c(x)$ and Overall Size of the Complex $H$.** Variation of the functional $\Delta\Phi$ (eq 18) with respect to unknown function $c(x)$ leads to the following condition for the local equilibrium within the complex,[19b]

$$c(x)[\delta g\{c(x)\}/\delta c(x)] - g\{c(x)\} = 0 \quad (19)$$

to give

$$v_{eff}c(x)^2 + 2w_{eff}c(x)^3 - 3f^3/[16\pi^2 a^2 c(x)x^4] = 0 \quad (20)$$

Equation 20 ensures the constant value of the osmotic pressure (or, equivalently, the conservation of the chemical potential of solvent molecules within the complex).[19b]

**1. Good Solvent Conditions.** Under the conditions that the pair contacts between monomers dominate, $v_{eff} \gg c(x)w_{eff}$, the contribution of the ternary contacts is negligible, and the second term in eq 20 can be omitted. As a result, the polymer density profile $c(x)$ is given by

$$c(x) \cong f^{2/3} a^{-2/3} (v_{eff})^{-1/3} x^{-4/3} \quad (21)$$

The size of the corona is obtained by integrating $c(x)$ according to eq 12.[19,20] We find the equilibrium size of the micelle−polyion complex to be

$$H_+ \cong af^{1/5}N^{3/5}(v_{eff}/a^3)^{1/5} \quad (22)$$

where the subscript (+) indicates good solvent conditions. Here and below, the numerical coefficients are omitted if not specified otherwise.

**2. Θ Solvent Conditions.** Inferior solvent strength, $|v_{eff}| \ll c(x)w_{eff}$, leads to the dominance of ternary contacts. We can neglect the contribution of the pair contacts in eq 20, and the polymer density profile scales as

$$c(x) \cong f^{1/2}a^{-1/2}(w_{eff})^{-1/4}x^{-1} \quad (23)$$

The overall size of the complex is given by

$$H_\Theta \cong af^{1/4}N^{1/2}(w_{eff}/a^6)^{1/8} \quad (24)$$

where subscript (Θ) indicates Θ solvent conditions.

The crossover between the two dependences for the polymer density profiles occurs at distance

$$x^* \cong (f/a)^{1/2}(w_{eff})^{3/4}(v_{eff})^{-1} \quad (25)$$

At distances $x \ll x^*$, the polymer density profile is given by eq 23 whereas at distances $x \gg x^*$, the distribution of polymer is determined by eq 21. Therefore, under good solvent conditions, the inner part of the polymer density profile is still determined by the ternary contacts between monomers. This, however, does not change dependence (22) for the overall size of the complex provided that $x^* \ll H_+$. By substituting the corresponding expressions 22 and 25, we find the lower boundary for the range of good solvent conditions,

$$v_{eff}/a^3 \cong f^{1/4}N^{-1/2}(w_{eff}/a^6)^{5/8} \quad (26)$$

**3. Poor Solvent Conditions.** A further decrease in solvent strength leads to the collapse of the complex due to the attractive pair interactions. Under these conditions, the stretching of branches can be neglected. Correspondingly, the equilibrium concentration of polymer within the complex is determined by the balance of attractive pair contacts and repulsive ternary interactions to give

$$c(x) \cong |v_{eff}|/w_{eff} \quad (27)$$

The overall size of the collapsed complex scales as

$$H_- \cong (Nw_{eff}/|v_{eff}|)^{1/3} \quad (28)$$

where subscript (−) indicates poor solvent conditions. Similar to the case of good solvent conditions, the distribution of polymer within the inner part of the complex (closer to the core of micelle) is governed by the ternary contacts. That is, at distances $x < x^{**}$ where

$$x^{**} \cong (f/a)^{1/2}w_{eff}^{3/4}|v_{eff}|^{-1} \quad (29)$$

the polymer density profile is given by eq 23 whereas at distances $x \gg x^{**}$, the polymer distribution is given by eq 27. Scaling dependence (28) does not change, however, when $x^{**} \ll H_-$. This inequality determines the upper boundary for the range of collapsed complex conditions,

$$v_{eff}/a^3 \cong -f^{1/4}N^{-1/2}(w_{eff}/a^6)^{5/8} \quad (30)$$

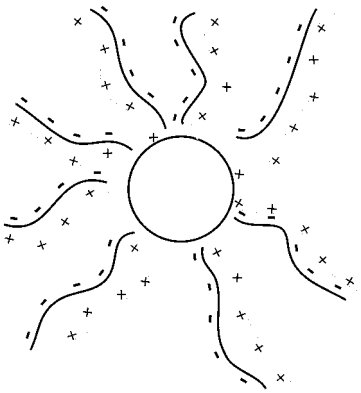

**Figure 1.** Representation of the complex formed between a cationic polymer micelle and a polyanion.

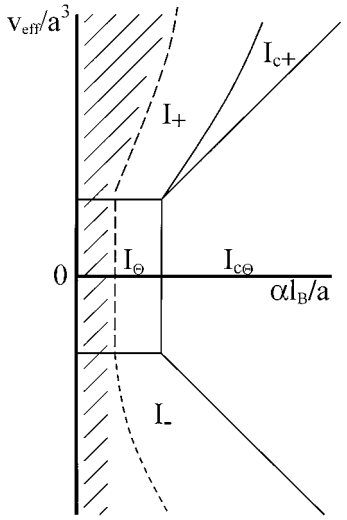


**Figure 2.** Diagram of states as a function of the effective second virial coefficient ($v_{eff}$) and the degree of ionization of the micelle corona (α).

**B. Diagram of States.** Our analysis indicates that in framework of the self-consistent-field model there are three different regimes for micelle−polyion complex. These regimes are delineated in the diagram of states of the complex in Figure 2 as $I_+$, $I_\Theta$, and $I_-$. The diagram is presented in the $v_{eff}/a^3$, $\alpha l_B/a$ coordinates. For simplicity, we focus here on the case of exact matching of the charge, $\alpha = \beta$. Under these conditions, the effective third virial coefficient $w_{eff}/a^6 = 8w/a^6 =$ constant (and we omit it from consideration), whereas the effective second virial coefficient $v_{eff}/a^3 = 4v + \chi$ can be changed due to variations in $v$ or $\chi$. When $v_{eff}/a^3 > f^{1/4}N^{-1/2}$, the complex is swollen by the repulsive pair contacts between monomers (region $I_+$ in Figure 2). When $|v_{eff}/a^3| < f^{1/4}N^{-1/2}$, the complex is swollen by the repulsive ternary contacts (region $I_\Theta$ in Figure 2). Finally, when $v_{eff}/a^3 < -f^{1/4}N^{-1/2}$, the complex is stabilized by the attractive pair and repulsive ternary contacts between monomers (region $I_-$ in Figure 2).

The regimes $I_+$, $I_\Theta$, and $I_-$ describe complexes where the charge on the micelle is compensated by the bound polyions despite unfavorable nonelectrostatic interactions between the polyions and the branches of micelle. Decreases in charge on the micelle and polyions destabilize the complex, and at small values of α (and $\beta$), the nonelectrostatic interactions destroy the complex. That is, the polyions are released from the complex and are substituted by the mobile counterions. (The size of the

free micelle is then given by eq 1.) Under the conditions of a good or a Θ solvent, the threshold of complex formation can be estimated by equating the sizes of micelle in the complex (eqs 22 and 24) and in the free state (eq 1). We obtain respectively $v_{eff}/a^3 = f^{-1}N^2\alpha^{5/2}$ and $\alpha l_B/a = f^{1/2}N^{-1}$ (the dashed line in Figure 2). To the left of this line, the micelles do not form complexes with polyions (shaded area). In a poor solvent, the situation is more complicated and will be considered elsewhere. Here, the dashed line in Figure 2 indicates the boundary between the swollen and the collapsed states of an individual micelle, $v/a^3 = \alpha^{-1/2}$.

In addition to regions $I_+$, $I_\Theta$, and $I_-$, the diagram contains also two novel regimes $I_{c+}$ and $I_{c\Theta}$. We discuss them below.

**1. Charge Correlations Induced Collapse.** Up to now we have exploited a self-consistent-field model of the complex. In this model the distributions of charge due to all the components are smoothed and averaged. The spatial correlations between the locations of different charges are ignored. We now take into account the correlations between charges following the ideas developed earlier.[21]

In the framework of our model, the oppositely charged groups of the micelle and polyion do not form irreversible links, and the micelle−polyion complex can be envisioned as a gas of pointlike charges. The electrostatic interactions between oppositely charged species in such a system lead to a correlation contribution ($\Delta F_{corr}$) to the total free energy ($\Delta\Phi$) of the system,[22]

$$\Delta F_{corr}/kT = -8(\pi l_B)^{3/2}/3\int_R^H x^2[\alpha c(x) + \beta n(x)]^{3/2}\,dx = -8(\pi l_B)^{3/2}/3\int_R^H x^2[2\alpha c(x)]^{3/2}\,dx = 4\pi\int_R^H x^2 g_{corr}\{c(x)\}\,dx \quad (31)$$

Here, $g_{corr}\{c(x)\}$ is the contribution to the density of the free energy of complex due to the correlation attraction between charges. This contribution to the total density $g\{c(x)\}$ gives rise to the additional term in eq 27, which is now modified as

$$c(x)^2 v_{eff} + 2c(x)^3 w_{eff} - \pi^{1/2}(2\alpha l_B)^{3/2}c(x)^{3/2}/3 = 3f^3/(16\pi^2 a^2 c(x)^2 x^4) \quad (32)$$

Equation 32 indicates that, in addition to the regimes discussed above, one can find a collapsed complex where the repulsive pair or ternary monomer−monomer interactions are balanced by the correlation attraction between charges.

Under the conditions of a good solvent, the balance of binary contacts with the charge correlation term (that is, the balance of the first and the third terms on the left-hand side of eq 32) gives

$$c(x) \cong (\alpha l_B)^3/v_{eff}^2 \quad (33)$$

(recall that numerical coefficients are omitted in all the scaling dependences).

If, however, we consider the complex as a semidilute solution of polymer and incorporate the monomer−monomer correlations according to scaling concepts[23] (that is, assume that $\delta f_{mix}a^{-3}/\delta c(x) \cong (v_{eff}/a^3)^{3/4}[c(x)a^{-3}]^{5/4}$), we arrive at a different power law dependence

$$c(x) \cong (\alpha l_B/a)^2/v_{eff} \quad (34)$$

The overall size of the complex is given by

$$H_{c+} \cong [fNv_{eff}/(\alpha l_B/a)^2]^{1/3} \quad (35)$$

where subscript (c+) indicates that the collapsed state of the complex is stabilized by the repulsive pair contacts and the correlation attraction. Below we use eqs 34 and 35 to describe the structure of complex in the $I_{c+}$ regime. We recall that incorporation of scaling corrections for starlike polymers swollen in good solvents does not change the dependence described by eq 22 for the overall size of the complex in the $I_+$ regime (see discussion in ref 20b for more details).

Balancing the ternary contacts with the charge correlation term in eq 32 gives for the equilibrium polymer concentration

$$c(x) \cong \alpha l_B/(w_{eff})^{2/3} \quad (36)$$

Here, the overall size of the complex scales as

$$H_{c\Theta} \cong [fNw_{eff}^{2/3}/(\alpha l_B)]^{1/3} \quad (37)$$

where subscript (cΘ) indicates the collapsed state of the complex stabilized by the repulsive ternary contacts and the correlation attraction between charges.

The collapsed states of micelle−polyion complex induced by the correlation attraction between charges are delineated in the diagram of states (Figure 2) as $I_{c+}$ and $I_{c\Theta}$ regions. The boundaries between these regimes and the regimes $I_+$, $I_\Theta$, and $I_-$ can be obtained by equating the corresponding expressions for the complex size H. We recollect that the diagram in Figure 2 is derived for the case of charge matching, $\alpha = \beta$, and any dependence on $w_{eff}$ is omitted. In addition to the already established boundaries $I_+$−$I_\Theta$ (eq 26) and $I_\Theta$−$I_-$ (eq 30), the other boundaries are given by

$$v_{eff}/a^3 \cong (\alpha l_B/a)^5 N^2 f^{-1} \qquad I_+ - I_{c+} \quad (38)$$

$$v_{eff}/a^3 \cong (\alpha l_B/a) \qquad I_{c+} - I_{c\Theta} \quad (39)$$

$$v_{eff}/a^3 \cong -(\alpha l_B/a) \qquad I_- - I_{c\Theta} \quad (40)$$

$$\alpha l_B/a \cong N^{-1/2} f^{1/4} \qquad I_{c\Theta} - I_\Theta \quad (41)$$

The diagram indicates that the effects of correlation attraction become significant at relatively high degrees of ionization, $\alpha l_B/a > N^{-1/2}f^{1/4}$. For flexible polymers with $l_B/a \approx 1$ and for a micelle with $f = 100$ and $N = 100$ the transition to the correlations induced collapsed state of the complex is expected at $\alpha > 0.3-0.4$.

We note that the collapsed states of micelle−polyion complex (regions $I_-$, $I_{c+}$, and $I_{c\Theta}$) are characterized by the positive surface free energy associated with the sharp boundary between the body of the complex and the pure solvent. This positive surface energy promotes the attraction between complexes and their possible precipitation from the solution. The thermodynamically stable water-soluble complexes are expected in regions $I_+$ and $I_\Theta$ where the boundary between the complex and the solvent is smoothed.

## V. Numerical Self-Consistent-Field (SCF) Theory

The findings of our analytical theory formulated in the previous section are based on certain simplifying

assumptions (total release of small counterions, local electroneutrality of the complex, equal stretching of the branches, etc.) We now employ a more refined numerical SCF model to check these assumptions and to supplement our analytical results with more precise numerical data. Because of its inherent nature, the numerical SCF method does not account for the charge correlations within the complex (regions $I_{c+}$ and $I_{c\Theta}$ of the diagram in Figure 2). We therefore focus on the mean-field regions $I_+$, $I_\Theta$, and $I_-$.

The well-known Scheutjens−Fleer formalism employs a lattice model of the system. In our case, it is a spherically symmetric shell of concentric layers of total thickness $D$. (The thickness of a single layer is chosen as a unit length and is equal to the size of monomer.) The dense micelle core of thickness $R$ is located in the center of the shell and is impermeable for the branches of micelle and polyions. We kept fixed the following parameters in all our calculations: $R/a = 10$, $f = 100$, $N = 100$, and $D/a = 100$. (These values are similar to the properties of the PVP−PS micelles studied in ref 14.) In some cases discussed later $N = 300$ was used. For a "salt-free system" the solution was composed primarily of polyions and their counterions although to ensure convergence of the calculations extremely small concentrations of salt ions were also present. The total number of polyion monomers added is designated by the symbol $\Theta$ and typically is 12 000, which slightly exceeds the number of monomer units in the corona ($fN$ = 10 000). The strength of electrostatic interactions in the system was varied by changes in the degrees of ionization of the micelle ($\alpha$) and the polyion ($\beta$). The nonelectrostatic interactions were described by the values of Flory−Huggins parameters of polymer−polymer and polymer−solvent interactions, $\chi$ and $\chi_{ps}$, respectively.

The numerical SCF method searches for the minimum of the total free energy of the system. As a result, it finds the equilibrium distributions of all the components (corona chains, polyions, salt ions, etc.) and determines the distribution of electric field on the level of the Poisson−Boltzmann formalism. The fundamentals of the numerical SCF method can be found in ref 24, and a description of the particular scheme used in this work was presented in ref 25. A similar approach was employed earlier to study the dilute and semidilute solutions of charged starlike polymer.[25b]

**A. Individual Micelle.** We start with a single micelle immersed in a water solution. Figure 3 demonstrates the equilibrium polymer density profiles of corona chains, $c(x)$, as a function of distance $x$ from the core of micelle at various degrees of ionization $\alpha$. If $\alpha$ is equal to zero, the micelle is electroneutral, and the polymer density profile in the corona reflects the features of a neutral spherical brush in a good solvent.[26] That is, one finds a rapid decay in the polymer density at small distances from the core, which becomes "parabolic-like" at the periphery of the corona. Because of relatively short branches (in this calculation $N = 100$), the two regimes are not so distinct.[27] Even a small increase in $\alpha$ leads to additional swelling of the corona, and the shape of the polymer density profile changes. For $\alpha > 0.1$ the $c(x)$ profile rapidly becomes very similar to the $\alpha = 1$ fully charged case (intermediate values of $\alpha$ not shown for clarity.

**B. Micelle−Polyion Complex.** The addition of oppositely charged polyions to the system leads to the formation of a micelle−polyion complex. The polyions

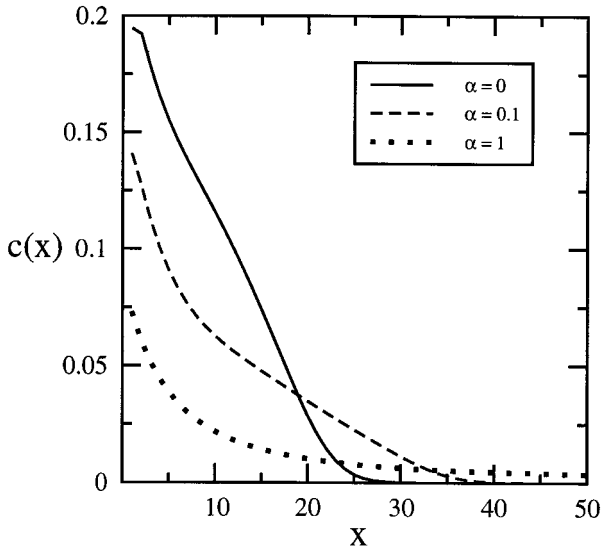


**Figure 3.** Polymer micelle corona density profile ($c(x)$) as a function of distance from the micelle core for the indicated degrees of ionization ($\alpha$) (all for $\chi_{ps} = 0$, a good solvent and no added polyion, $\Theta = 0$).

penetrate the corona of the micelle and shield the repulsion between the branches, leading to the release of small ions to the surrounding solution. As was discussed above, the major driving force for polyion−micelle complexation is the displacement of small counterions by the polyion with the concomitant gain of entropy. To test this idea, we carried out some calculations in which different numbers of polyion monomers were added (e.g., variable $\Theta$ value) at a constant number of segments per polyion ($P$). In Figure 4a we present the corona profile ($c(x)$) for $\Theta$ in the range 0−16 000 (for $\alpha = 1$ and $P = 100$). The initial few additions of polyion causes the profile to contract from the polyion-free case ($\Theta = 0$), but then the profile steadily expands as $\Theta$ increases, up to the point that the number of polyion segments equals the number of corona segments ($\Theta$ = 10 000), with essentially no change thereafter. These SCF calculations clearly demonstrated that variations in the total amount of added polyelectrolyte did not affect the structure of complex provided that $\Theta$ was sufficient to compensate the total charge on the micelle. These results are also in agreement with the analytical model.

The effect of $P$ can be also examined by calculating $\Theta_{excess}$, defined by

$$\Theta_{excess} = \frac{4\pi}{V_{total}} \int_R^D (n(x) - n_{bulk}) x^2 \, dx \qquad (42)$$

where $n_{bulk}$ is the concentration of the polyion near the outer edges of the spherical compartment that contains the micelle ($V_{total}$ is the total volume of the compartment) (see Figure 4b). For $P > 20$ $\Theta_{excess}$ approaches 10 000, meaning that almost all charge compensation is the result of the polyion inside the micelle corona (Figure 4b).[28] Therefore, we do not expect any significant effect of $P$ unless it is much less than $N$ (recall that $N$ = 100 for our calculations). This is in qualitative agreement with the experimental results in ref 14 and our analytical model. Almost all the original small anions have been expelled, as their excess drops to nearly zero (not shown because there is nearly complete charge compensation when small ions are included; see

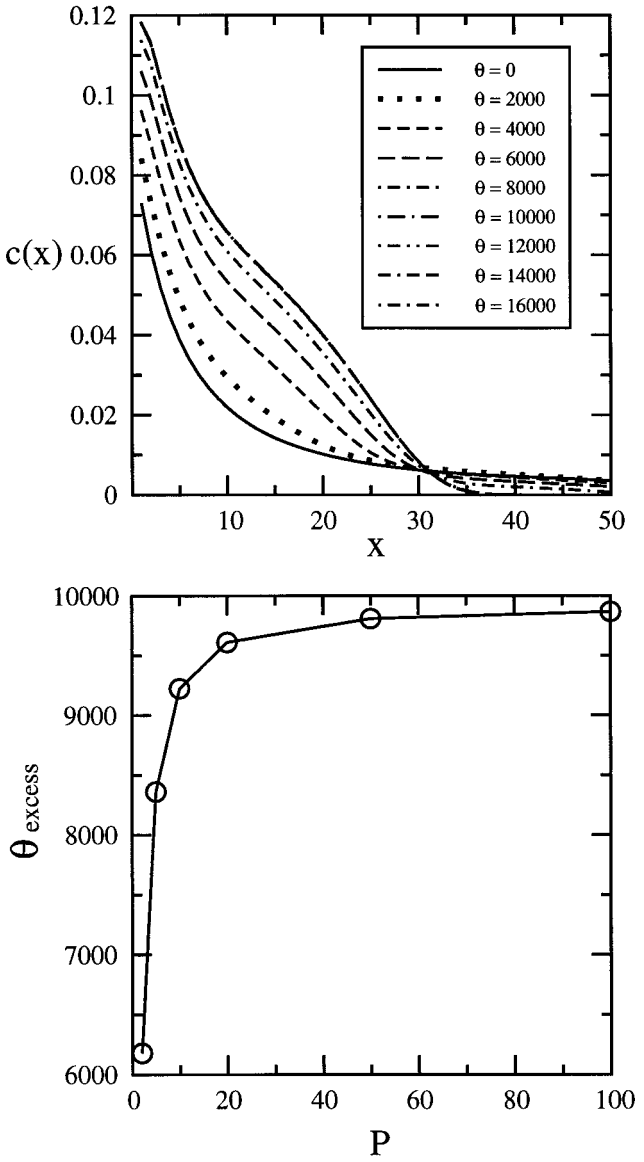


**Figure 4.** (a) Polymer micelle corona density profile ($c(x)$) for different concentrations of the polyion (values of Θ indicate the total number of polyion segments). The number of segments on each polyion ($P$) is 100, and $\alpha = \beta = 1$. Since the number of segments in the corona is 10 000 ($fN$) charge compensation by the polyion is possible for Θ = 10 000. (b) Plot of the excess polyion in the micelle corona ($\Theta_{excess}$) as defined by eq 42 as a function of the number of segments on the polyion ($P$) (all for Θ = 12 000). As $\Theta_{excess}$ approaches 10 000, all counterions in the corona have been replaced by the polyion.

later discussion). There was no hint of charge or mass overcompensation, as expected from a SCF calculation.

We now explore the structure of micelle−polyion complex as a function of the charge density on the chains and the solvent quality.

**1. Size of Micelle−Polyion Complex.** The size of the complex $H_1$ was calculated as the first moment of the polymer density distribution $c(x)$,

$$H_1 = \int_R x^3 c(x)\,dx / \int_R^H x^2 c(x)\,dx = 4\pi(fNa^3)^{-1}\int_R x^3 c(x)\,dx \quad (43)$$

The degree of ionization of the polyion was kept equal to that of the micelle, $\beta = \alpha$. The quality of the solvent

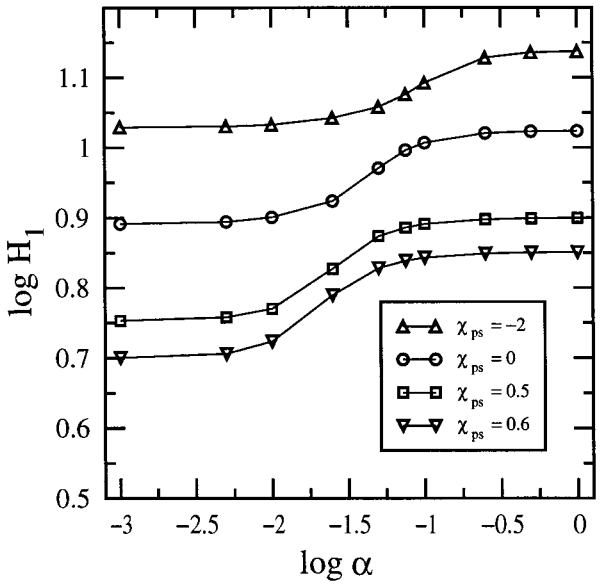


**Figure 5.** Plot of the polymer micelle thickness ($H_1$) as a function of corona ionization (α) for the indicated values of $\chi_{ps}$ ($\chi = 0$, $P = 100$, Θ = 12 000 for all calculations).

was varied from very good ($\chi_{ps} = -2$ and $\chi_{ps} = 0$) to a Θ solvent ($\chi_{ps} = 0.5$) and then to a poor solvent ($\chi_{ps} = 0.6$) (recall that $\chi$ is taken to be equal to 0). Figure 5 displays the behavior of $H_1$ as a function of the degree of ionization α (in logarithmic coordinates) for different values of $\chi_{ps}$. The curves in Figure 5 indicate that at relatively high values of α the size of the complex is almost unaffected by decreases in α. This is in agreement with the prediction of the analytical model, as the size of the complex is determined by the effective virial coefficients of monomer−monomer interactions, $v_{eff}$ and $w_{eff}$ (eqs 16 and 17). When the degrees of ionization of the micelle and of the polyion coincide ($\beta = \alpha$), the values of $v_{eff}$ and $w_{eff}$ do not depend on α. Therefore, the size of the complex does not change with variations in α. Inferior solvent strength leads, however, to a decrease in $v_{eff}$, and the size of complex diminishes.

Further decreases in α destroy the complex, and the size of micelle gradually approaches the value for a neutral micelle (α = 0). As is seen from Figure 5, each curve has two "plateau" regions: one corresponding to a complex at larger α and the other to an individual neutral micelle for small α. There is also a transition region that corresponds to the gradual disruption of the complex. In our scaling model, the transition region is associated with the boundary of the shaded area in Figure 2 where the complex does not form. Under Θ solvent conditions ($\chi_{ps} = 0.5$) the position of this boundary (dashed line in the diagram in Figure 2) is given by $\alpha l_B/a = f^{1/2}N^{-1}$ (see the discussion of the diagram of states). For our set of parameters ($f = 100$, $N = 100$, and $l_B/a = 1$) the scaling model predicts (within the accuracy of a numerical coefficient on the order of unity) α = 0.1 for this boundary. We see from Figure 5 that for $\chi_{ps} = 0.5$ (corresponding to a Θ solvent) the transition region occurs close to α = 0.1. Under good solvent conditions ($\chi = 0, -2$), the transition region shifts to the larger values of α. This is also in agreement with the diagram of states: the dashed line shifts to the right with increases in $v_{eff}$ (see Figure 2).

According to our analytical model, the size of the micelle−polyion complex is governed by the values of $v_{eff}$ and $w_{eff}$. To check this prediction, we performed the

calculations not only for the symmetric case ($\alpha = \beta$) but varied $\alpha$ and $\beta$ separately and also changed the parameters of polymer−solvent and polymer−polymer interaction, $\chi_{ps}$ and $\chi$. (These quantities are not equal to each other in general for the calculations discussed here.) The values of parameters were varied as follows: $0.4 < \alpha, \beta < 0.6$; $-2 < \chi_{ps} < 0.6$, $-0.1 < \chi < 0.5$. This allowed us to vary both $v_{eff}$ and $w_{eff}$ and to calculate $H_1(v_{eff},w_{eff})$ (see eq 43).

We will discuss the general behavior of the size of the micelle−polyion complex in terms of the reduced size $Y = H_1(v_{eff},w_{eff})/H_1(v_{eff}=0,w_{eff})$. $H_1(v_{eff}=0,w_{eff})$ is the size of micelle−polyion complex under the "effective" $\Theta$ conditions, $v_{eff} = 0$. For neutral starlike polymers in $\Theta$ solvents, ternary contacts between monomers lead to swelling of the star with respect to the Gaussian size ($=aN^{1/2}$).[20] In the limit of strong stretching, $H_1 \gg aN^{1/2}$, the size of the star in a $\Theta$ solvent is given by $H_1(v_{eff}=0,w_{eff}) \cong aN^{1/2}w_{eff}^{1/8}f^{1/4}$.[20b] Swelling of the starlike polymer under the conditions $v_{eff} > 0$ can be considered along the lines of the Flory theory[17] (see also ref 20b). That is, the free energy $F$ of the starlike polymer as a function of the swelling ratio of the branch $\gamma = H_1/aN^{1/2}$ can be described as

$$F/kT = 3f(\gamma^2/2 - \ln \gamma) + v_{eff}f^2N^{1/2}\gamma^{-3} + w_{eff}f^3\gamma^{-6} \quad (44)$$

Here, the first term arises from the stretching of the $f$ branches of the star (each branch is considered as an individual Gaussian chain stretched from its unperturbed size $aN^{1/2}$ up to $H_1$), whereas the second and the third terms are due to the pair and ternary contacts between monomers (which are assumed to be spread uniformly within the volume of the star). The numerical coefficients are omitted. Minimization of the free energy $F$ with respect to $\gamma$ gives an equation for the swelling ratio of the star,

$$\gamma^8 - \gamma^6 = \gamma^3(v_{eff}fN^{1/2}) + w_{eff}f^2 \quad (45)$$

By substituting $\gamma = Y(w_{eff}^{1/8}f^{1/4})$ in eq 45, we arrive at the following equation for $Y$,

$$Y^5 - Y^{-3} - Y^3(w_{eff}^{1/4}f^{1/2})^{-1} = (v_{eff}N^{1/2})/(w_{eff}^{5/8}f^{1/4}) = Z \quad (46)$$

When the number of branches ($f$) and the third virial coefficient ($w_{eff}$) are fixed, eq 46 predicts a universal dependence, $Y = Y(Z)$. When, however, $w_{eff}$ is varied, the deviations from the universal curve $Y = Y(Z)$ due to the third term on the left-hand side in eq 46 could be noticeable. For example, when $Z = 0$ and $w_{eff}^{1/4}f^{1/2} \gg 1$, the reduced size $Y$ scales as $(Y - 1) = (w_{eff}^{1/4}f^{1/2})^{-1}$.

Figure 6 demonstrates the reduced size of the complex $Y = H_1(v_{eff},w_{eff})/H_1(v_{eff}=0,w_{eff})$ vs $Z = (v_{eff}N^{1/2})/(w_{eff}^{5/8}f^{1/4})$ calculated for the values of $f = 100$ and $N = 300$. (This larger value of $N$ was selected to accentuate the effect of chain stretching in the corona.) The value of $H_1(v_{eff}=0,w_{eff})$ was determined as $H_1(v_{eff}=0,w_{eff}) = aN^{1/2}w_{eff}^{1/8}f^{1/4} = H_1(\chi_{ps}=1/2, \chi=0, \alpha=\beta=0.5)\,[(1+\alpha/\beta)/2]^{3/8}$. As is seen from Figure 6, the data points localize around the master curve. The diamonds correspond to the symmetric case, $\alpha = \beta$, and for the values of $\alpha = 0.4$, 0.5, and 0.6 the data points lie virtually on top of each other. We note that when $\alpha = \beta$, $w_{eff} = 8w$ and $v_{eff} = 4v + \chi$ (eqs 17 and 16), and variations in $\alpha$ do not change the values of $w_{eff}$ and $v_{eff}$. For values of $\alpha < \beta$ the data points are shifted above the master curve while for $\alpha > \beta$ they are shifted below the master curve. These systematic deviations are not large but still noticeable. Equation 46 indicates that due to the third term on the left-hand side, the reduced size $Y$ should increase (with respect to the symmetric case) when $\alpha < \beta$ and decrease when $\alpha > \beta$. We anticipate that an increase in the number $f$ of branches will reduce the effect of the third (nonuniversal) term in eq 46 and diminish the deviations from the master curve. We note that eq 46 does not take into account the final size of the core. This approximation is valid when the size of the corona $H_1$ exceeds noticeably the size of the core $R$, $H_1 \gg R$. Therefore, increases in length of the branch $N$ would also diminish the deviations from the master curve.

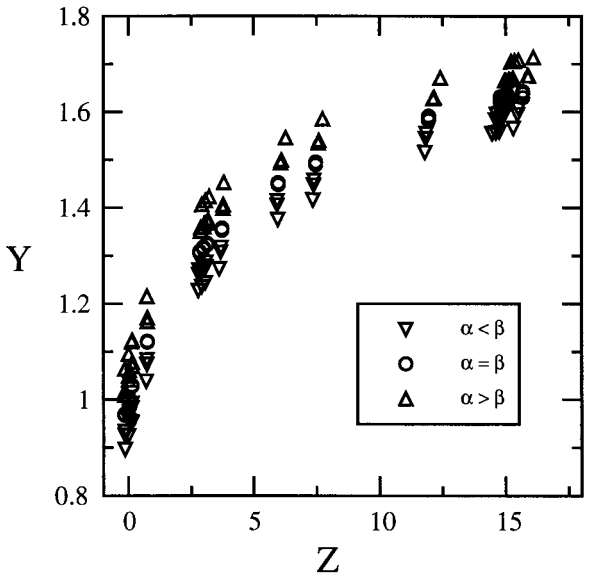


**Figure 6.** Plot of scaled and normalized micelle thickness $Y = H_1(v_{eff},w_{eff})/H_1(v_{eff}=0,w_{eff})$ vs the swelling parameter $Z = (v_{eff}N^{1/2})/(w_{eff}^{5/8}f^{1/4})$ (see text). The parameters $P$ and $\Theta$ are the same as in Figure 5, but a variety of $\chi_{ps}$ and $\chi$ values were used. For these calculations we picked $N = 300$ to accentuate chain stretching in the corona.

**2. Distribution of Polymer in the Complex.** Figure 7a demonstrates the effect of charging on the corona structure for the symmetric ($\alpha = \beta$) micelle−polyion complex in the $\Theta$ solvent ($\chi_{ps} = 0.5$). For weak charging ($\alpha = 0.01$), the complex is not stable, and the corona density profile ($c(x)$, see Figure 7a) is typical of a neutral micelle corona (see Figure 3). For values of $\alpha$ in the range 0.05−0.10 the complex is formed, and further increases in $\alpha$ do not lead to noticeable change in the corona profile within the complex. (We recollect that according to Figure 5 the transition region of micelle−polyion complex in the $\Theta$ solvent is located around $\alpha = 0.1$.) The $c(x)$ profile in the complex demonstrates the convex and concave curvature that is typical of neutral micelles.

Figure 7b presents the polyion density profiles ($n(x)$) for different charge densities. For $\alpha > 0.05$ the distributions of polyions are very similar to each other, and the micelle−polyion complex is thermodynamically stable. At $\alpha = 0.05$, the polyions start to leave the complex, and at $\alpha = 0.01$ the complex is destroyed. (The concentration of polyion inside the micelle is only slightly higher than in the surrounding solution.)

Figure 8 demonstrates how the free ends of the corona branches are distributed throughout the complex for the

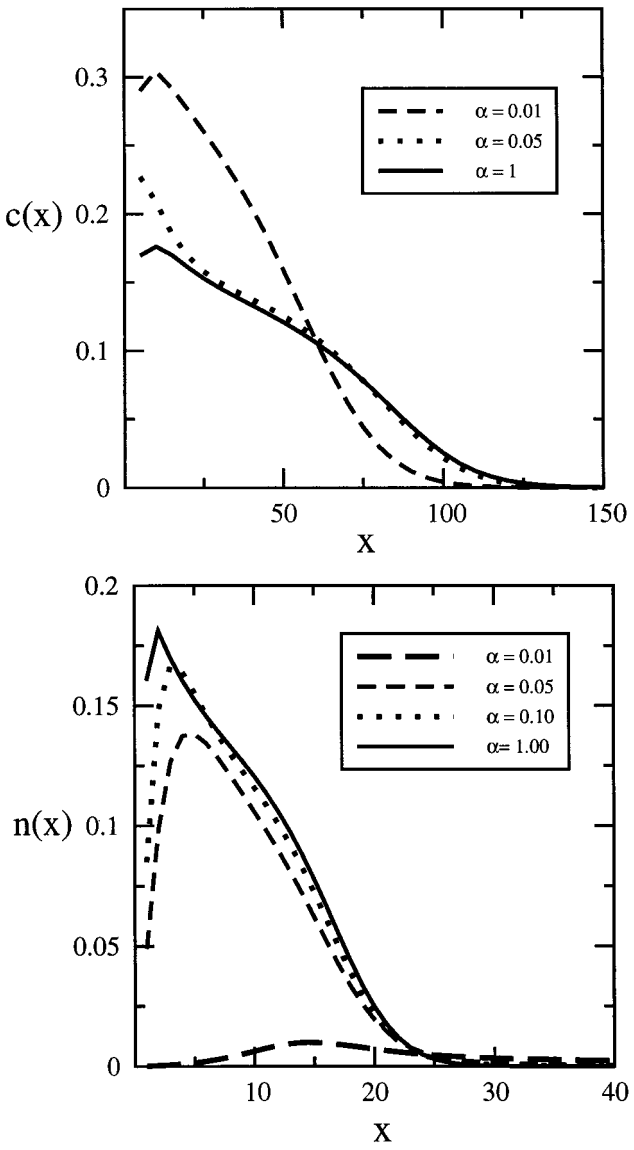


**Figure 7.** (a) Corona density plot ($c(x)$) and (b) the polyion density plot ($n(x)$) for the symmetric ($\alpha = \beta$) micelle−polyion complex in a Θ solvent for different values of α ($\chi_{ps} = 0.5$ and $\chi = 0$, $P = 100$, $\Theta = 12\,000$ for all calculations).

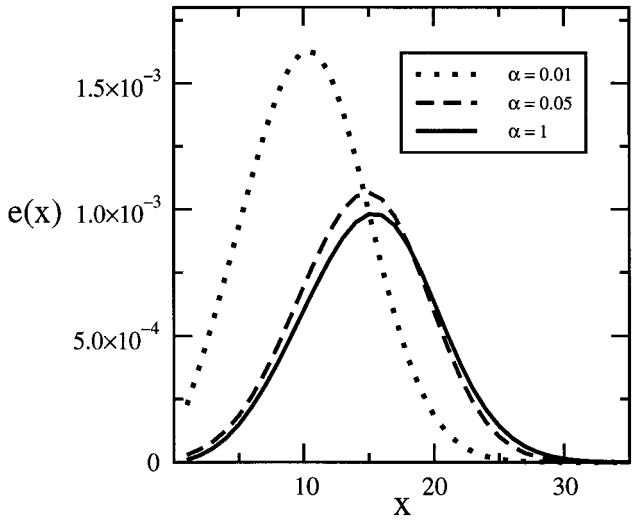


**Figure 8.** Density profile of the corona end groups ($e(x)$) for the same set of parameters as in Figure 7.

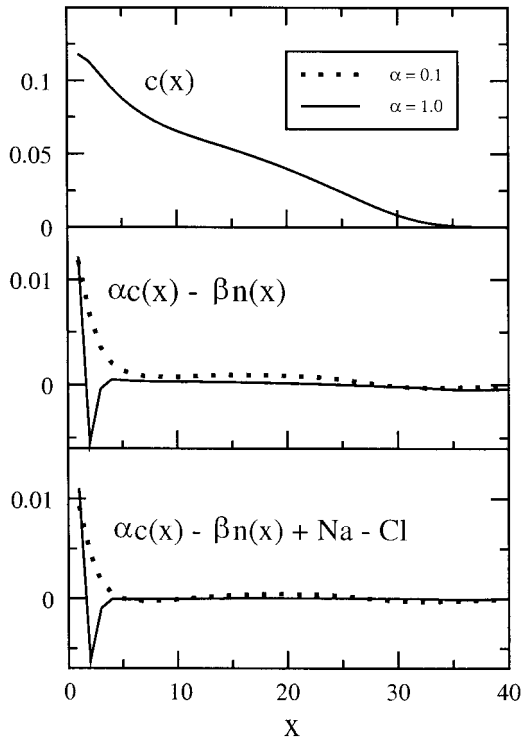


**Figure 9.** Net corona−polyion charge density ($\rho(x) = \alpha c(x) - \beta n(x)$) and total charge density ($\rho_T(x) = \alpha c(x) - \beta n(x) + c_{Na^+}(x) - c_{Cl^-}(x)$) compared with the $c(x)$ profile for for $\alpha = 1$, for the same set of parameters as Figure 7 (note that $c(x)$ is essentially identical for α from 0.1 to 1).

same values of parameters as in Figure 7. As is seen from Figure 8, for the chosen set of parameters the free ends of the branches are widely distributed within the complex. In micelles with larger branches and in better solvents ($\chi_{ps} < 0.5$), the free ends become more localized at the periphery of the corona (not shown in Figure 8), but the distribution is still rather broad.

**3. Distribution of Charge in the Complex.** Figure 9 displays the distribution of the net corona−polyion charge density, $\rho(x) = \alpha c(x) - \beta n(x)$, or the total charge density (lower panel) (the parameters are the same as in Figure 7). The deviation from electroneutrality at small $x$ is a typical double-layer effect within a few lattice constants of the interface. As is seen from Figure 9, there is some expulsion of the polyions from the complex for $\alpha = 0.1$, which leads to an increase in $\rho(x)$. Even for relatively short branches ($N = 100$ for these calculations), the local electroneutrality condition (eq 14) seems to be a reasonable approximation to describe the micelle−polyion complexes.

**4. Effect of Charge Distribution of the Polyion on the Structure of the Complex.** We now focus on how the distribution of charges along the backbone of the polyion affects the features of the micelle−polyion complex. According to our scaling model, the structure of the micelle−polyion complex is not sensitive to the specific charge distribution on the polyion but is determined by its average degree of ionization $\beta$. To check this prediction, we performed the SCF calculations for a micelle with $f = 100$, $N = 100$, and degree of ionization $\alpha = 0.5$, forming complexes with the following polyions:

Case 1: A uniformly charged homopolymer of $P = 100$ monomers with $\beta = 0.5$ (i.e. identical parameters used for the calculations discussed earlier).

Case 2: A diblock copolymer with a noncharged block of 50 monomers with $\beta = 0$ and a charged block of 50

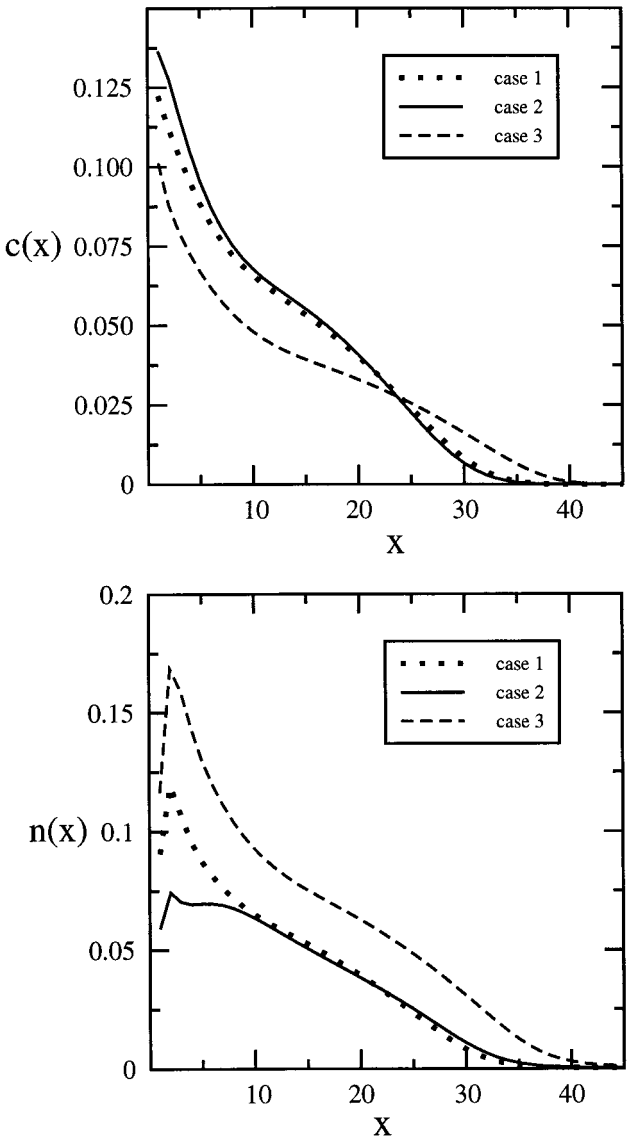


**Figure 10.** (a) $c(x)$ for the homogeneously charged (case 1) and diblock (case 2) polymers (both with $\beta = 0.5$ and $P = 100$) and the polymer with every fourth monomer carrying a full charge ($\beta = 0.25$ and $P = 200$) (case 3). (b) $n(x)$ for the same cases as (a) (other parameters as in Figure 7).

monomers with $\beta = 1$. In this case, the length of the polyion (100) and its average degree of ionization (0.5) are the same as in case 1, but the charge along the polyion is distributed asymmetrically.

Case 3: A multiblock copolymer of $P = 200$ monomers with a repeating block consisting of one charged monomer ($\beta = 1$) and three noncharged monomers ($\beta = 0$). In this case, the total charge on the chain (50) is the same as in cases 1 and 2, but the average degree of ionization, $\beta = 0.25$, is halved.

The amounts of added polyion were sufficient to compensate the charge on the micelle ($\Theta = 12\,000$ in cases 1 and 2, and $\Theta = 24\,000$ in case 3).

Figure 10 demonstrates the distribution of monomers for the corona chains ($c(x)$) and the polyion ($n(x)$) for these three cases. As is seen from Figure 10a, in cases 1 and 2 the polymer density profiles for the corona chains are virtually identical. For uniformly charged polyion (case 1), $c(x)$ is somewhat lower near the core of the micelle and is only slightly larger in the peripheral part of the corona than for diblock polyion (case 2). We

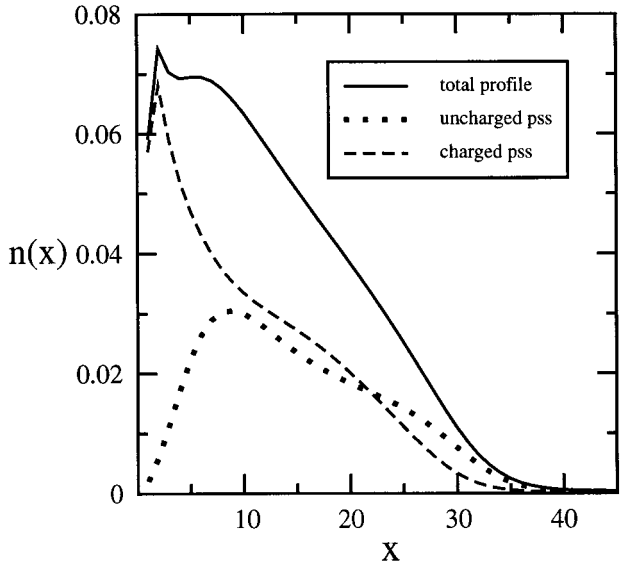


**Figure 11.** Distribution of the charged and uncharged blocks of the diblock polyion and the total polyion distribution ($n(x)$). The latter is the same as case 3 of Figure 10b.

note that even such a small difference between the two profiles in the peripheral part is sufficient to compensate the noticeable difference near the core of micelle because the total charge at distance $x$ is proportional to $x^2$. In case 3 the polymer density is noticeably lower, and the complex is more swollen. This is not surprising because the micelle−polyion complex contains more neutral monomers, leading to an increase in the effective virial coefficients, $v_{\text{eff}}$ and $w_{\text{eff}}$, according to eqs 16 and 17.

In Figure 10b we compare the polyion density profiles, $n(x)$, for the three different types of polyions. The density profile for case 3 lies noticeably above the two other curves due to the increased amount of neutral monomers in the complex. In the context of an SCF theory this is the only way to achieve mass overcompensation; i.e., excess neutral polymer is dragged into the corona by the charged portion of the polymer. Comparison of the curves for case 1 and 2 indicates that whereas in the peripheral part of the corona the two density profiles are very close, near the core of micelle, the density profile of the diblock polyion demonstrates a nonmonotonic behavior. Thus, the blocklike distribution of the charge on polyion can influence the detailed structure of the interior of the complex.

In Figure 11 we plot the spatial distributions of the charged and of the neutral monomers of the diblock polyion in the corona of micelle. The density profiles of the charged and the uncharged monomers demonstrate qualitatively similar features. Both density profiles exhibit a maximum and have an adjacent shoulder. However, the charged monomers concentrate closer to the higher charge density that exists near the core, and the density profile exhibits a relatively steep maximum near the core. Obviously, the noncharged blocks do not participate in the charge compensation, and they are shifted to the more dilute peripheral part of the corona. (If the neutral blocks were cut from the charged ones, they would be totally expelled from the micelle.) Because of the connectivity of the blocks in the diblock polyion, there is only partial separation of the two density profiles.

Therefore, we conclude that the overall size of the micelle−polyion complex is not strongly affected by the

specific charge distribution on the polyion, but the detailed internal structure of the complex could change noticeably.

## VI. Discussion

The results of this work indicate that a thermodynamically stable micelle−polyion complex is formed when the charges on the branches of micelle corona are compensated by the oppositely charged polyions that are "absorbed" by the corona. The driving force for this process is the release of counterions from the corona of the micelle into the bulk solution. Because of the substitution of small counterions by macroions, the gain in translational entropy of the system is about $QkT$ per micelle where $Q$ is the total micelle charge. SCF calculations indicate that "local electroneutrality" is achieved by nearly complete replacement of the small counterions by the polyion, in agreement with the analytical theory. There is very little influence of the length of the polyion on this process once the polyion is larger than approximately 20 units (for a corona chain length of 100, although we believe this will be a general result). There are deviations from electroneutrality near the micelle core−corona interface which are typical double-layer effects.

The analytical theory developed in this paper employs the "volume" approximation to describe the complex. That is, the free energy of the micelle−polyion complex reflects the contributions only from the body of the micelle and does not account for any effects associated with the surface of the complex. We also ignore the possible conformational losses due to the absorbed polyions. By taking advantage of the local electroneutrality approximation, we described the equilibrium structure of the complex (its total size and the polymer density profiles in the corona) under a variety of conditions. The major conclusion is that the equilibrium structure of the complex is governed by the effective second and third virial coefficients of monomer−monomer interactions, $v_{\text{eff}} = v(1 + \alpha/\beta)^2 + \alpha\chi/\beta$ and $w_{\text{eff}} = w(1 + \alpha/\beta)^3$. These effective virial coefficients can be mediated by variations in the solvent strength (which determines the value of actual second virial coefficient $v$), degrees of ionization, $\alpha$ and $\beta$, and the incompatibility of the polymers (through the Flory−Huggins parameter, $\chi$). Depending on the relative values of $v_{\text{eff}}$ and $w_{\text{eff}}$, the characteristics of the micelle−polyion complex are described by different asymptotical laws. The scaling diagram of the states describes different regimes of the complex behavior and delineates the range of its thermodynamic stability.

We note that our analytical model does not take into account the electrostatic stiffening of the corona chains and the polyion, an effect which becomes significant for highly charged species with $\alpha \cong 1$ and $\beta \cong 1$ (the same holds for the numerical SCF model as well). As is known (see, for example, ref 29 and references therein), the electrostatic stiffening of a highly charged polyelectrolyte is governed by the intrinsic flexibility of polymer and the electrostatic screening length $\kappa^{-1}$. For flexible polymers with $a \cong l_B$, the electrostatic stiffening becomes important when $\alpha > (a\kappa)^{3/2}$.[29] As follows from the diagram of the states, at high values of $\alpha$ (for $\beta = \alpha$) the micelle−polyion complex is found in the collapsed state induced by the correlation attraction between the charges. Here, the screening length $\kappa^{-1}$ is determined as $\kappa^{-1} \cong (l_B \alpha c)^{-1/2}$,[21b] where $c$ is average concentration of polymer in the micelle−polyion complex (eqs 34 and 36). That is, in the collapsed complex with $\alpha = \beta$, the electrostatic screening length scales as $(a\kappa)^{-1} \cong \alpha^{-3/2}$ and as $(a\kappa)^{-1} \cong \alpha^{-1}$ in a good and a $\Theta$ solvent, respectively. Therefore, the electrostatic stiffening starts to effect the structure of the micelle−polyion complex only when $\alpha \geq 1$.

It follows from our analysis that the charged micelle with bare charge $Q = \alpha fN$ can bind an amount of polyion of the same total charge. That is, the mass or number of monomers of the bound polyion, $M$, is given by $M = \alpha fN/\beta$. When the polyion is ionized to a lesser extent than the branches of the micelle, one can expect a noticeable mass overcompensation of the complex, i.e., $M/fN = \alpha/\beta > 1$. This was also verified by explicit SCF calculations. It remains an open question how much neutral polymer can be dragged into a charged corona as a function of $\alpha$, $\beta$, and $\alpha/\beta$.

Recent experiments[14] performed on micelles composed of polystyrene−*block*-poly(2-vinylpyridine) interacting with sodium poly(styrenesulfonate) (PSS) in water solutions indicated huge mass overcompensation of the micelle−polyion complex. The pH of the solution was low enough (pH = 1) to protonate the pyridine groups so that the degree of ionization of the poly(2-vinylpyridine) block (corona block of the micelle) could approach unity ($\alpha = 1$) in principle.[30] The degree of sulfonation of PSS chains was close to 94%, and the molecular weight of the samples varied in the range 5K−800K. Static light scattering (SLS) measurements indicated that the apparent molecular mass of the micelle−PSS complex increased with the concentration of micelles in the solution while holding the PSS concentration constant. This was attributed to the formation of PSS bridges between the micelles. To eliminate this effect, the SLS data were extrapolated to zero micelle concentration. The observations demonstrated that at vanishing concentration of micelles in the solution the amount of bound PSS units was on the order of 4.7−5.5 per pyridine group. The effect of the molecular weight of PSS in the investigated range (5K−800K) was minor. The weak dependence of the apparent mass of the micelle−PSS complex on the length of PSS chains is in agreement with our analytical theory.

The experimental observations of ref 14 can be interpreted in different ways. A lower degree of ionization of the added polyelectrolyte with respect to that of a micelle can lead to mass overcompensation according to the ratio $\alpha/\beta > 1$ per monomer of the corona block. Although the degree of sulfonation of the PSS molecules was reported to be high (=94%), the effective dielectric constant in the interior of the corona−polyion complex could be substantially lower than in pure water, thereby encouraging the formation of ion pairs between the polyion and $H^+$ counterions at pH = 1. (This is equivalent to raising the $pK_a$ of the PSS.) Therefore, it is possible that the actual degree of ionization of the sulfonated groups in the PSS molecules could be decreased, which yields a PSS/PVP ratio of $\alpha/\beta$.

Another possible explanation for the phenomena observed in ref 14 is charge inversion of the micelle−polyion complex. The problem of overcharging of ionized objects by oppositely charged polyelectrolytes has attracted considerable attention recently.[29,32−37] The origin of the overcharging is attributed to particular configurational aspects[32−34] and/or the strong correlations between screening ions.[29,35,37] Up to the moment, the

models used to study overcharging were limited to impermeable charged interfaces (spherical or planar surfaces). In this case, the polyelectrolyte binds to the surface forming a double electric layer. (The charges due to the polymer are separated from the opposite charge on the interface.) In the case of the micelle−polyion complex, the interface is the relatively diffuse corona of the micelle, which is accessible to the oppositely charged flexible polymer. The appearance of overcharging on the scale of the whole corona seems unlikely because of the huge electrostatic energy penalty associated with such an interface. However, the outer boundary of the complex could be overcharged due to the loops produced by the absorbed polyions. The system would be then reminiscent of a spherical colloid particle of size $H$ covered with loops of polyelectrolyte. Overcharging of a spherical charged particle by a flexible polyelectrolyte in a dilute solution was considered in ref 32. By using an analogy with the quantum theory of the atom, Gurovitch and Sens showed that the maximal overcharging of a pointlike particle with charge $Q$ may be estimated to be $15/6 = 2.5$.[32] If micelle−polyion complex is envisioned as charged only at the outer boundary with the surface charge $Q' < Q$, the overcharging $2.5Q'/Q$ is still much less than observed experimental values.[14] Numerical simulations employed a model of spherical impermeable macroion to describe the charged micelle.[34] Obviously, this model cannot account for the softness of corona. A recent publication addresses the problem of interaction of charged objects with multivalent (macro) ions using the ideas of strongly correlated liquids.[35] In this approach, the origin of overcharging is the strong correlation between macroions (see also ref 36). However, in the formalism of ref 35, the charged micelle would be still modeled as a rigid sphere of fixed size, and the internal structure of the micelle (which, we believe, is a key issue in the formation of these complexes) remains outside of the considerations of this paper. An attempt to consider interaction of polyions with an oppositely charged interface of finite thickness was carried out in ref 38. The interface was modeled by a planar layer of finite thickness and had the total surface charge less than the surface charge due to the polyions. A fraction of the polyions was embedded in this layer to shield the charge of the interface, while the rest were stretched and protruded into the solution. Overcharging of the interface in this case (absorption of extra polyions into the interfacial layer) occurred due to the electrostatic repulsion between protruding polyions. Though the results of ref 38 are not directly applicable to micelle−polyion complexes, they enhance our understanding of the overcharged systems that could appear under, say, nonequilibrium conditions. We note that the nonequilibrium features of micelle−polyion aggregates could be also responsible for the observed mass overcompensation of the PVP/PS−PSS complexes studied in ref 14.

Finally, we would like to emphasize that all the results of this paper hold in the salt-free solutions (or solutions for which the salt-controlled Debye radius $r_D$ exceeds the size $H$ of the micelle−polyion complex, $r_D \gg H$). Decreases in $r_D$ will lead to the screening of electrostatic attraction between micelle and polyions and finally destabilization of the complex. We will address the effect of added salt in a separate publication. It is also interesting to consider the case of an annealed polyion in the presence of acid or base, which will be the subject of later theoretical study.

**Acknowledgment.** Financial support from the National Science Foundation (Grant DMR-9973300) is greatly acknowledged. We are also grateful to Dr. Frans Leemakers and Dr. Jan van Male at Wageningen University (The Netherlands) for fruitful discussions and help in the numerical SCF calculations on charged polymers. E.B.Z. acknowledges comments of Prof. M. Rubinstein and Dr. A. Dobrynin at the University of North Carolina on the role of charge correlation attraction in micelle−polyion complexes.

## Appendix

We have to minimize the functional of the free energy $\Delta\Phi = \Delta W_{el} + \Delta F_{mix} + \Delta F_{str}$,

$$\Delta\Phi/kT = l_B/2\int_R^H r^{-2}\,dr\,\{\int_R^r x^2\,dx\,[\alpha c(x) - \beta n(x)]\}^2 + 4\pi\int_R^H x^2\{v[n(x)+c(x)]^2 + w[n(x)+c(x)]^3 + \chi c(x)\,n(x)\}\,dx + 3f^3/8\pi a^2\int_R^H 1/[c(x)x^2]\,dx \quad \text{(A1)}$$

with respect to two unknown functions $n(x)$ and $c(x)$ under the constraints

$$4\pi\int_R^H c(x)x^2\,dx = fN \quad \text{(A2)}$$

and

$$4\pi\int_R^H n(x)x^2\,dx = M \quad \text{(A3)}$$

where $M$ is the total amount of polyion in the micelle−polyion complex.

To incorporate the constraints (eqs A2 and A3), we search for the extremum of functional

$$\Delta\Phi_1/kT = \Delta\Phi/kT - 4\pi\lambda\int_R^H c(x)x^2\,dx - 4\pi\mu\int_R^H n(x)x^2\,dx \quad \text{(A4)}$$

where $\lambda$ and $\mu$ are the indefinite Lagrange multipliers. Variation of $\Delta\Phi_1/kT$ yields

$$\delta\Delta\Phi_1/kT = \int_R^H \delta c(x)\,dx\,\{l_B x^2\alpha\int_x^H r^{-2}u(r)\,dr + 4\pi a^3x^2[2v(c(x)+n(x)) + 3w(c(x)+n(x))^2 + \chi n(x) - \lambda] - 3f^2/[8\pi a^2c(x)^2x^2]\} + \int_R^H \delta n(x)\times dx\,\{-l_B x^2\beta\int_x^H r^{-2}u(r)\,dr + 4\pi a^3x^2[2v(c(x)+n(x)) + 3w(c(x)+n(x))^2 + \chi c(x) - \mu]\} \quad \text{(A5)}$$

where function $u(r)$ is given by

$$u(r) = \int_R^r t^2[\alpha c(t) - \beta n(t)]\,dt \quad \text{(A6)}$$

Expressions in figure brackets in eq A5 should be equal to zero at the minimum of functional $\Delta\Phi_1/kT$. We therefore arrive to the following equations for $n(x)$ and $c(x)$,

$$4\pi[2v[c(x)+n(x)] + 3w[c(x)+n(x)]^2 + \chi n(x)] + l_B\alpha\int_x^H r^{-2}u(r)\,dr - 3f^2/[8\pi a^2c(x)^2x^4] = 4\pi\lambda \quad \text{(A7)}$$

$$4\pi[2v[c(x) + n(x)] + 3w[c(x) + n(x)]^2 + \chi c(x)] - l_B\beta\int_x^H r^{-2}u(r)\,dr = 4\pi\mu \quad \text{(A8)}$$

By adding and subtracting eqs A7 and A8, we obtain

$$4\pi\{2v[c(x) + n(x)](\alpha + \beta) + 3w[c(x) + n(x)]^2(\alpha + \beta) + \chi[\alpha c(x) + \beta n(x)]\} - 3\beta\phi^2/[8\pi a^2 c(x)^2 x^4] = 4\pi(\lambda\beta + \mu\alpha) = 4\pi\Lambda_1 \quad \text{(A9)}$$

$$4\pi\chi[n(x) - c(x)] + l_B(\alpha + \beta)\int_x^H r^{-2}u(r)\,dr - 3f^2/[8\pi a^2 c(x)^2 x^4] = 4\pi(\lambda - \mu) = 4\pi\Lambda_2 \quad \text{(A10)}$$

Under conditions of a good solvent ($v > 0$, $w = 0$), eq A9 is a linear equation with respect to $n(x)$. By solving it, we express the polyion density profile, $n(x)$, as a function of the corona density profile, $c(x)$, as

$$n(x) = \{3\beta f^2/[32\pi^2 a^2 c(x)^2 x^4] + \Lambda_1\}/[2v(\alpha + \beta) + \chi\beta] - c(x)[2v(\alpha + \beta) + \chi\alpha]/[2v(\alpha + \beta) + \chi\beta] \quad \text{(A11)}$$

Under conditions of a Θ or a poor solvent, eq A9 is a quadratic equation with respect to $n(x)$ that could be also solved analytically. However, the corresponding calculations become too cumbersome, and we proceed below with the case of a good solvent ($w = 0$). By substituting expression A11 for $n(x)$ in eq A10, we obtain

$$6vf^2/\{8\pi a^2 c(x)^2 x^4[2v(\alpha + \beta) + \chi\beta]\} + 4\pi\chi c(x)[4v + \chi]/[2v(\alpha + \beta) + \chi\beta] = l_B\int_x^H r^{-2}u(r)\,dr + \Lambda \quad \text{(A12)}$$

where Λ is a new constant. Equation A12 is an integral equation with respect to $c(x)$. To simplify further analysis, we reduce it to a differential equation of the second order. First differentiation of eq A12 with respect to $x$ leads to

$$6vf^2/\{8\pi a^2[2v(\alpha + \beta) + \chi\beta]\}\,d[x^{-4}c(x)^{-2}]/dx + 4\pi\chi[4v + \chi]/[2v(\alpha + \beta) + \chi\beta]\,d[c(x)]/dx = -l_B u(x)x^{-2} \quad \text{(A13)}$$

Second differentiation of eq A13 with respect to $x$ gives

$$6vf^2/\{8\pi a^2[2v(\alpha + \beta) + \chi\beta]\}\,d\{x^2\,d[x^{-4}c(x)^{-2}]/dx\}/dx + 4\pi\chi[4v + \chi]/[2v(\alpha + \beta) + \chi\beta]\,d\{x^2\,d[c(x)]/dx\}/dx = -l_B x^2[\alpha c(x) - \beta n(x)] \quad \text{(A14)}$$

By substituting expression A11 for $n(x)$ in eq A14, we obtain the final equation for polymer density profile $c(x)$,

$$3vf^2(4\pi a^2 l_B\beta^2 x^2)^{-1}\,d\{x^2\,d[x^{-4}c(x)^{-2}]/dx\}/dx + 4\pi\chi[4v + \chi](\beta x)^{-2}(l_B)^{-1}\,d\{x^2\,dc(x)/dx\}/dx + c(x)[2v(1 + \alpha/\beta)^2 + 2\alpha\chi/\beta] - 3f^3/[32\pi^2 a^2 c(x)^2 x^4] - \Lambda_1/\beta = 0 \quad \text{(A15)}$$

When the micelle−polyion complex is not deformed (its size $H$ corresponds to the minimum of the free energy functional $\Delta\Phi(H)$), the constant on the rhs in eq A15 can be neglected provided that $\mu$ is not too low. (We recall that $\mu$ is the chemical potential per monomer of the polyion in the bulk solution and can be mediated by variations in polyion bulk concentration.) Then the structure of complex is not sensitive to the bulk concentration of polyion and is totally governed by the micelle−polyion interactions. Under these conditions, the polymer density profile in the complex is determined by the approximate equation

$$3vf^2(4\pi a^2 l_B\beta^2 x^2)^{-1}\,d\{x^2\,d(x^{-4}c^{-2})/dx\}/dx + 4\pi\chi(4v + \chi)(\beta x)^{-2}(l_B)^{-1}\,d\{x^2\,dc/dx\}/dx + c[2v(1 + \alpha/\beta)^2 + 2\alpha\chi/\beta] - 3f^2/(32\pi^2 a^2 c^2 x^4) \approx 0 \quad \text{(A16)}$$

We now proceed with the scaling analysis of eq A16. Namely, we search for solution of eq A16 in the form

$$c(x) = Ax^\gamma \quad \text{(A17)}$$

where $A(f,v,\alpha,\beta,\chi)$ is a function which does not depend on distance $x$, and $\gamma$ is an unknown exponent. By substituting eq A17 into eq A16, we obtain

$$x^{3\gamma+4}A\{[2v(\alpha + \beta)^2 + 2\alpha\beta\chi] + 4\pi\chi(4v + \chi)\gamma(\gamma + 1)x^{-2}(l_B)^{-1}\} = 3f^3(4\pi a^2 A^2)^{-1}\{\beta^2/8\pi - (2\gamma + 3)(2\gamma + 4)v(l_B)^{-1}x^{-2}\} \quad \text{(A18)}$$

As is seen from eq A18, the first terms in figure brackets do not depend on $x$ whereas the second terms in figure brackets decrease as $x^{-2}$. Therefore, the second terms can be neglected at not too small distances $x$ from the center of micelle. (We note that $x > R$ where $R$ is radius of the core.) By retaining only the first terms in figure brackets and omitting the numerical coefficients, we obtain

$$\gamma = -4/3 \qquad A = f^{2/3}a^{-2/3}(v_{\text{eff}})^{-1/3} \quad \text{(A19)}$$

By substituting expressions A19 in eq A17, we obtain the scaling expression for the polymer density profile,

$$c(x) = f^{2/3}a^{-2/3}(v_{\text{eff}})^{-1/3}x^{-4/3} \quad \text{(A20)}$$

where

$$v_{\text{eff}} = v(1 + \alpha/\beta)^2 + \alpha\chi/\beta \quad \text{(A21)}$$

is the effective second virial coefficient of monomer−monomer interactions. We therefore find that under the conditions of a good solvent the electrostatic attraction between oppositely charged polymers (the corona forming blocks and the polyion) is much stronger than the nonelectrostatic repulsion between monomers, and locally, the complex is almost electroneutral. That is,

$$\alpha c(x) \approx \beta n(x) \quad \text{(A22)}$$

The local electroneutrality approximation (eq A22) allows us to envision the micelle−polyion complex as a neutral system with the renormalized virial coefficients of monomer−monomer interactions. We use this approximation to consider the conformations of the micelle−polyion complex in a wide range of solvent strengths.

## References and Notes

(1) Decher, G.; Hong, J. G.; Schmitt, J. *Thin Solid Films* **1992**, *210−211*, 831.

(2) Ferreira, M.; Cheung, J. H.; Rubner, M. F. *Thin Solid Films* **1994**, *244*, 806. Ferreira, M.; Rubner, M. F. *Macromolecules* **1995**, *28*, 7107.
(3) Napper, D. *Polymeric Stabilization of Colloid Dispersions*; Academic Press: London, 1983.
(4) Radler, J. O.; Koltover, L.; Salditt, T.; Safinya, C. R. *Science* **1997**, *275*, 810.
(5) Grunstein, M. *Nature* **1997**, *389*, 349.
(6) (a) Harada, A.; Kataoka, K. *Science* **1999**, *283*, 65. (b) Gohy, J.-F.; Varshney, S. K.; Antoun, S.; Jerome, R. *Macromolecules* **2000**, *33*, 9298.
(7) Marko, J. F.; Rabin, Y. *Macromolecules* **1992**, *25*, 1503. Wittmer, J.; Joanny, J. F. *Macromolecules* **1993**, *26*, 2691. Dan, N.; Tirrell, M. *Macromolecules* **1993**, *26*, 4310. Shusharina, N. P.; Nyrkova, I. A.; Khokhlov, A. R. *Macromolecules* **1996**, *29*, 3167.
(8) Tuzar, Z.; Kratochvil, P. *Surf. Colloid Sci.* **1993**, *15*, 1.
(9) Zhang, L.; Eisenberg, A. *Science* **1995**, *268*, 1728.
(10) Zhang, L.; Barlow, R. J.; Eisenberg, A. *Macromolecules* **1995**, *28*, 6055.
(11) Cao, T.; Munk, P.; Ramireddy, C.; Tuzar, Z.; Webber, S. E. *Macromolecules* **1991**, *24*, 6300.
(12) Kataoka, K. *J. Macromol. Sci., Pure Appl. Chem.* **1994**, *A31*, 1759. Rolland, A.; O'Mullane, J.; Goddard, P.; Brookman; Petrak, K. *J. Appl. Polym. Sci.* **1992**, *44*, 1195. Kiserow, D. Prochazka, K.; Ramireddy, Ch.; Tuzar, Z.; Munk, P.; Webber, S. E. *Macromolecules* **1992**, *25*, 461.
(13) Groenewegen, W.; Lapp, A.; Egelhaaf, S. U.; van der Maarel, J. R. C. *Macromolecules* **2000**, *33*, 4080. Groenewegen, W.; Egelhaaf, S. U.; Lapp, A.; van der Maarel, J. R. C. *Macromolecules* **2000**, *33*, 3283. van der Maarel, J. R. C.; Groenewegen, W.; Egelhaaf, S. U.; Lapp, A. *Macromolecules*, in press.
(14) Talingting, M. R.; Voigt, U.; Munk, P.; Webber, S. E. *Macromolecules* **2000**, *33*, 9612.
(15) Bohmer, M. R.; Evers, O. A.; Scheutjens, J. M. H. M. *Macromolecules* **1990**, *23*, 2288.
(16) Borisov, O. V. *J. Phys. II* **1996**, *1*, 19.
(17) Flory, P. J. *Principles of Polymer Chemistry*; Cornell University Press: Ithaca, NY, 1953.
(18) Semenov, A. N. *Sov. Phys. JETP* **1985**, *61*, 733.
(19) (a) Zhulina, E. B. *Macromolecules* **1993**, *26*, 6273. (b) Misra, S.; Mattice, W. L.; Napper, D. H. *Macromolecules* **1994**, *27*, 7090.
(20) (a) Daoud, M.; Cotton, J. P. *J. Phys. (Paris)* **1982**, *43*, 531. (b) Birshtein, T. M.; Zhulina, E. B. *Polymer* **1994**, *25*, 1453.
(21) (a) Higgs, P. G.; Joanny, J. F. *J. Chem. Phys.* **1991**, *94*, 1543. (b) Dobrynin, A. V.; Rubinshtein, M. *J. Phys. II* **1995**, *5*, 677.
(22) Landau, L. D, Lifshitz, E. M. *Statistical Physics, Part 1*; Pergamon Press: New York, 1980.
(23) De Gennes, P. J. *Scaling Concepts in Polymer Physics*; Cornell University Press: Ithaca, NY, 1979.
(24) Fleer, G. J.; Cohen-Stuart, M. A.; Scheutjens, J. M. H. M.; Cosgrove, T.; Vincent, B. *Polymers at Interfaces*; Chapman and Hall: London, 1993.
(25) (a) van Male, J. SFBOX:C++ implementation of Scheutjens−Fleer self-consistent-field formalism for inhomogeneous molecular systems, Wageningen, 2000. (b) Klein Walterink, J.; Leermakers, F. A. M.; Fleer, G. J.; Koopal, L. K.; Zhulina, E. B.; Borisov, O. V. *Macromolecules* **1999**, *32*, 2365.
(26) Wijmans, C. M.; Zhulina, E. B. *Macromolecules* **1993**, *26*, 7214.
(27) As was demonstrated earlier,[26] increases in the length of the branch, for $N$ from 200 to 500, make these two parts of the polymer density profile rather pronounced. The initial part of the profile is then described by a power law, whereas the external part of the profile (where the branches are found in the "planarlike" geometry) approaches the parabola expected for planar brushes in good solvents.
(28) Note that $\Theta_{excess}$ underestimates the fraction of charge compensation from the polyion because there is additional polyion inside the micelle corona, given roughly by $n_{bulk}V_{coron}$ (where $V_{coron}$ is the volume of the corona region).
(29) Netz, R. R.; Joanny, J. F. *Macromolecules* **1999**, *32*, 9013.
(30) The state of protonation for the corona for this system is a more complex issue than the quenched polyelectrolyte considered in this paper as it is expected that $\alpha$ will be a strong function of distance from the micelle core (see ref 20). However, it is plausible that complexation with PSS enhances the degree of protonation of the poly(2-vinylpyridine) corona such that $\alpha$ increases significantly.
(31) Borisov, O. V.; Zhulina, E. B. *Eur. Phys. J.* **1998**, *B4*, 205.
(32) Gurovitch, E.; Sens, P. *Phys. Rev. Lett.* **1999**, *82*, 339.
(33) Mateescu, E. M.; Jeppesen, C.; Pincus, P. *Europhys. Lett.* **1999**, *46*, 493.
(34) Wallen, T.; Linse, P. *Langmuir* **1996**, *12*, 305.
(35) Nguyen, T. T.; Grosberg, A. Yu.; Shklovskii, B. I. *J. Chem. Phys.* **2000**, *113*, 1110.
(36) Park, S. Y.; Bruinsma, R. F.; Gelbart, W. M. *Europhys. Lett.* **1999**, *46*, 454.
(37) Dobrynin, A. V. *J. Chem. Phys.*, in press.
(38) Zhulina, E. B.; Borisov, O. V.; van Male, J.; Leemakers, F. A. M. *Langmui*r, in press.

MA010399R